

# Line formation in Be star circumstellar disks<sup>\*,\*\*</sup>

## Shear broadening, shell absorption, stellar obscuration and rotational parameter

W. Hummel<sup>1</sup> and M. Vrancken<sup>2</sup>

<sup>1</sup> Institut für Astronomie und Astrophysik und Universitätssternwarte München, Scheinerstrasse 1, 81673 München, Germany

<sup>2</sup> Royal Observatory of Belgium, Ringlaan 3, 1180 Brussel, Belgium

Received 29 March 1999 / Accepted 28 April 2000

**Abstract.** We improve the theory of Horne & Marsh on shear broadening in accretion disks of CVs and adapt it to Be star circumstellar disks. Stellar obscuration and shell absorption are taken into account in detail. It is shown that shell absorption is already present in those emission lines where the central depression does not drop below the stellar continuum. The model profiles are fitted to observed symmetric  $H\alpha$  net emission lines with low equivalent width. The derived disk radii range from  $R_d = 5.3R_*$  to  $R_d = 18R_*$  and the surface emissivity varies as  $\sim R^{-m}$  with  $1.6 < m < 3.5$ . The comparison between model profiles of rotational parameter  $j > \frac{1}{2}$  with the optically thick  $H\alpha$  profile of HR 5440 rules out the range of  $j > \frac{1}{2}$ . This can be understood by the lack of velocity shear in the outer disk regions. We conclude that Keplerian rotation ( $j = \frac{1}{2}$ ) is a valid approximation.

**Key words:** line: formation – line: profiles – stars: circumstellar matter – stars: emission-line, Be

### 1. Introduction

Be stars are fast rotating early-type emission line stars. It is generally assumed that both line and continuum emission originate in a rotating disk-like envelope (see e.g. Smith et al. 2000). This idea is supported by the observed correlation between the stellar projected rotational velocity  $v \sin i$  and the width of the emission lines (Struve 1931).  $H\alpha$  emission line profiles of Be stars are usually complex but are understood qualitatively in terms of several broadening mechanisms and opacity effects (e.g. Hummel 2000).

For this reason, metallic lines as those of Fe II are to be preferred when deriving kinematical constraints of the circumstellar

disk since scattering smears out the kinematical information in the  $H\alpha$  emission profiles. However  $H\alpha$  line profiles of Be stars with low equivalent width are less complex. They do not show bumps in their wings implying that the vertical extension of the disk does not broaden the line profile due to multiple scattering. For this particular situation an elaborate 3D line transfer treatment (Hummel 1994) is no longer required. Electron scattering is also unimportant in low equivalent width  $H\alpha$  emission lines (Poeckert & Marlborough 1979). The emission line strength of  $H\alpha$  is empirically correlated with the emission line strength of metallic lines (Hanuschik 1987). Hence, for Be stars with low equivalent width in  $H\alpha$ , this is the only available emission line in the spectrum to be analyzed. It is therefore highly desirable to model low  $W_\alpha$  emission lines of Be stars to derive the kinematical properties and the distribution of the circumstellar emissivity.

Emission lines of large  $v \sin i$  Be stars usually show a deep depression between the double peak giving rise to large optical depth for high inclinations which indicates a flattened geometrical shape of the envelope. For some of these nearly edge-on systems the depression is lower than the stellar continuum (= *shell lines*) which is explained by a partial absorption of the central star by the circumstellar disk. The effect of stellar obscuration on optically thin emission lines has been studied by Hanuschik (1987). Sobolev (1960) and Hanuschik (1995, hereafter HK) calculated the shell-absorption as a purely absorption problem and for the limiting case of edge-on geometry ( $i = 90^\circ$ ).

Horne & Marsh (1986, hereafter HM) calculated optically thick emission lines of accretion disks in dwarf novae. HM found a simple expression for the local optical depth in a differentially rotating disk in terms of the Sobolev approach: line photons can leave a differentially moving gas in directions of largest Doppler gradients. Their model profiles show a deep ‘V’-shape between the double peak at inclinations  $i > 60^\circ$  with respect to model profiles in the optically thin limit. HM neglect the finite size of the central star. This is justified in dwarf novae where the central object is a white dwarf with a typical radius of  $R_* = 10^{-3} R_\odot$  and a neglectable continuum in the optical.

In this study we apply the method of Horne & Marsh to  $H\alpha$  emission lines and shell line of Be star circumstellar disks by taking the finite size of the central star and hence stellar

---

Send offprint requests to: W. Hummel

\* Based on observations collected at the German-Spanish Astronomical Center (DSAZ), Calar Alto, operated by the Max-Planck-Institut für Astronomie Heidelberg jointly with the Spanish National Commission for Astronomy

\*\* Based on observations collected at the Observatoire de Haute-Provence (OHP), CNRS, France

Correspondence to: hummel@usm.uni-muenchen.de

obscuration and shell absorption into account. In so far as we consider emission *and* absorption from circumstellar disks of Be stars at different inclinations.

The model extensions are described in Sect. 2 and a detailed study of the line profile shapes is performed in Sect. 3. In Sect. 4 we fit observed H $\alpha$  emission lines and derive disk parameters. In Sect. 5 we investigate the rotation law of Be stars. The results are discussed in Sect. 6 and conclusions are drawn in Sect. 7.

## 2. Basic model assumptions and equations

### 2.1. Shear broadening

Line photons that are trapped in an optically thick emission layer can escape more easily in directions along which the Keplerian shear flow provides large Doppler gradients. This anisotropy in the local emission pattern alters the shape of the global emission profile. Horne & Marsh (1986, their Eq. 10) found a simple analytic expression for the Doppler gradient along the line of sight:

$$V_{\text{sh}} = -\frac{H}{2R} V_{\text{K}} \sin i \tan i \sin \phi \cos \phi. \quad (1)$$

where  $i$  is the inclination,  $\phi$  is the azimuthal angle in the disk plane,  $H$  is the disk height,  $R$  is the radius and  $V_{\text{K}}$  is the local value of the Keplerian velocity. We generally follow Horne & Marsh, but allow for a radial gradient in the circumstellar density distribution ( $Z = z/R_*$ ;  $R = \sqrt{x^2 + y^2}/R_*$ ):

$$n(R, Z) = n_0 R^{-m} \exp \left[ -\frac{1}{2} \left( \frac{Z}{H(R)} \right)^2 \right]. \quad (2)$$

Values of  $m$  typical for Be star circumstellar disks range between [2...3.5] as derived from IR studies (e.g. Waters 1986). Therefore the surface density  $\Sigma$  varies with radius:

$$\Sigma(R) = \int n(R, Z) dZ = n_0 R^{-m} \sqrt{2\pi} H(R) R_* \quad (3)$$

where the scale height  $H(R)$  is given in units of the stellar radius by

$$H(R) = \frac{C_s}{V_{\text{K}}} R^{\frac{3}{2}}. \quad (4)$$

with  $C_s = \sqrt{\gamma R_g T_d}$  the sound speed ( $\gamma = \frac{5}{3}$  for mono-atomic gases;  $R_g$  is the universal gas constant) and  $V_{\text{K}} = \sqrt{GM_*/R_*}$  is the Keplerian velocity at  $R = R_*$ . The total number of absorbing particles is given by:

$$\begin{aligned} N_{\text{D}} &= \int_0^{2\pi} \int_{R_*}^{R_{\text{d}}} \Sigma(R) R dR d\phi \\ &= \frac{N_0}{\frac{7}{2} - m} \left[ R_{\text{d}}^{\frac{7}{2} - m} - 1 \right] \end{aligned} \quad (5)$$

where

$$N_0 = \frac{n_0 (2\pi)^{\frac{3}{2}} C_s R_*}{V_{\text{K}}}. \quad (6)$$

The final expression for the line optical depth  $\tau_\nu$  reads:

$$\tau_\nu = \frac{W(R)}{\cos i} \frac{\lambda_0}{\sqrt{2\pi} \Delta V} \exp \left[ -\frac{1}{2} \left( \frac{V - V_{\text{D}}(0)}{\Delta V} \right)^2 \right] \quad (7)$$

where the absorption equivalent width

$$W(R) = \frac{\pi e^2}{mc} f \Sigma(R) \quad (8)$$

becomes a function of radius as well as of the line profile width

$$\Delta V = \sqrt{\Delta V_{\text{th}}^2 + V_{\text{sh}}^2}. \quad (9)$$

For large inclinations Eq. (1) is no longer valid, since the radial velocity along the light path does no longer vary linearly. A reasonable upper inclination limit  $i < i_{\text{u}}$  for Eq. (1) would therefore be

$$\tan i_{\text{u}} \simeq \frac{R_{\text{d}}}{H(R_{\text{d}})}. \quad (10)$$

As is often assumed, we adopt  $T_{\text{d}} = \frac{2}{3} T_{\text{eff}}$  (Poeckert & Marlborough 1982, van Kerkwijk et al. 1995). The H $\alpha$  line source function

$$S^{\text{L}} = \frac{B_\nu(T_{\text{eff}})}{B_\nu(T_{\text{d}})} \approx 0.5 \quad (11)$$

is kept constant throughout the disk. Electron scattering is not taken into account, hence our approach is restricted to Be stars with low emission line strengths, for which the broadening of emission lines wings due to electron scattering can be neglected. For more details of the model we refer the reader to Horne & Marsh (1986), Marsh (1987) and Horne (1995).

### 2.2. Stellar obscuration and shell absorption

We now consider the part of the equatorial plane, that is obscured by the central star at a given inclination. For reasons of symmetry this obscured region (behind the star) in the equatorial plane has the same shape as the shell-region (in front of the star) and can be found by geometrical considerations:

$$R_{\text{o}}(\phi) = \frac{\sec i}{\sqrt{\cos^2 \phi + \sin^2 \phi \sec^2 i}} \quad (12)$$

where  $R_{\text{o}}$  is the obscuration radius (see Fig. 1),  $i$  is the inclination of the line-of-sight and  $\phi$  is the azimuthal angle in the equatorial plane of the disk measured counter-clockwise from the observers direction. For the particular inclination

$$\tan i_{\text{o}} = \frac{R_{\text{d}}}{R_*} \quad (13)$$

the obscuration  $R_{\text{o}}$  radius matches the disk radius  $R_{\text{d}}$ . For  $\phi = 0^\circ$  and for  $i = 90^\circ$  the obscuration region in the disk plane can be described by a stripe limited by  $-R_* < y < +R_*$  (HK). In the following we neglect limb darkening and gravitational darkening induced by the fast rotation of the central star. This also implies that we neglect the rotational flattening of the stellar

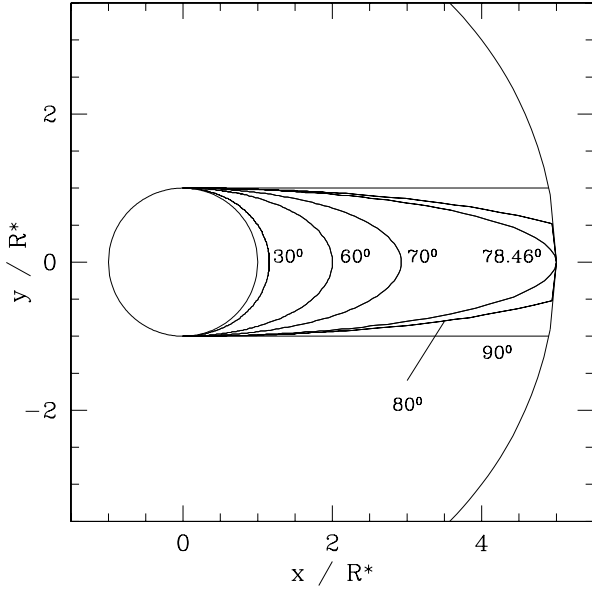


**Fig. 1.** Equatorial plane of a circumstellar disk with an outer disk radius of  $R_d = 5$ . The observer is located above the  $x > 0$  axis. The circumstellar shell region is defined by the disk area which is projected onto the stellar surface. This region increases with inclination and matches  $R_o = R_d$  at  $i = i_o = 78.46^\circ$ . For  $i = 90^\circ$  the total region between  $-1 < y < +1$  contributes to the shell area.

surface. The integrated specific intensity  $I_\nu$  (see HM Eq. (22)) has to be split according to the three different regions in the disk:

$$I_\nu = \cos i + \begin{cases} S^L(1 - e^{-\tau}) & : R > R_o \\ \zeta & : R < R_o \wedge \sin \phi < 0 \\ S^L(1 - e^{-\tau}) + \zeta e^{-\tau} & : R < R_o \wedge \sin \phi > 0 \end{cases} \quad (14)$$

The first line in Eq. (14) is the original expression of HM (1986; Eq. (14)) and is valid for photons emitted beyond the obscuration radius  $R > R_o$ . The second case represents that part of the circumstellar disk that is obscured by the star. The final case accounts for disk emission and absorption in the shell area located in front of the stellar surface. The normalization factor  $\zeta = \cos i / \pi$  gives the correct integral of the stellar radiation with respect to the inclined circumstellar disk. The  $\cos i$ -term in front of the bracket refers to the central part of the stellar surface which is neither absorbed nor obscures the circumstellar disk.

### 2.3. Large inclination effects

Since the scale height  $H(R)$  varies as  $\sim R^{1.5}$  it can be projected onto the stellar surface at large inclinations thus increasing the effective shell area (Hanuschik 1996). The projected  $H(R_d)$  is labeled as  $h_p$  in Fig. 2. This occurs at inclinations  $i > i_p$  with

$$\tan i_p = \frac{R_d - 1}{H(R_d)}. \quad (15)$$

For the modeling this effect must be taken into account only for large disks since only in this case  $H(R_d)$  becomes sufficiently large that  $i_p \leq i_u$ . The fraction of the stellar surface contributing to the shell effect becomes larger than approximated by Eq. (14). This geometric effect is parameterized via the projected height of  $H(R_d)$  at  $R_*$ . The shadow height  $h_p$  of  $H(R_d)$  at  $R_*$  is given by:

$$h_p = H(R_d) - (1 - R_d) \cot i \quad (16)$$

where  $h_p$  and  $H(R_d)$  are given in units of  $R_*$  and the observed fraction of the full stellar surface  $\pi$  obscured by  $H(R_d)$  is given by:

$$F(h_p) = \frac{\pi}{2} + h_p \sqrt{1 - h_p^2} - \arcsin h_p \quad (17)$$

with  $-1 \leq h_p \leq 1$  and  $0 \leq F(h_p) \leq \pi$ . We take this effect into account in Eq. (14) at large inclination when  $h_p(i) > 0$ .

### 2.4. Test calculation for pure shell profiles

We close this section by giving a calculation of pure shell profiles, neglecting the circumstellar emission ( $S^L = 0$ ). In Fig. 3 we show circumstellar shell profiles at different inclinations for a disk with  $R_d = 5$  and  $m = 2$ . The parameters are identical to those of HK. This includes  $M_* = 10M_\odot$ ,  $R_* = 7R_\odot$ , a maximum rotation velocity at the inner rim of the disk  $V_K = 521 \text{ km s}^{-1}$  an intrinsic broadening of  $\Delta V_{\text{th}} = 1.7 \text{ km s}^{-1}$  appropriate for Fe, a disk temperature of  $T_d = 10\,000 \text{ K}$  and a sound speed of  $C_s = 12 \text{ km s}^{-1}$ . The density  $n_0$  is chosen so that

$$\tau_{\text{HK}} = W(R_*) \frac{\lambda_0}{\sqrt{2\pi} C_s} = 10$$

(HK, his Eq. (8)). The shell profiles are given for inclinations  $i = 70^\circ, 72^\circ, 74^\circ, 76^\circ, 78^\circ, 80^\circ, 82^\circ, 84^\circ$  and  $86^\circ$  (solid profiles). The nominal upper inclination limit for this model is  $i_u = 87^\circ$  (see Eq. (10)), however the central thermal peak of the line profiles is already underestimated for  $i \geq 82^\circ$ . It is important to compare our model profiles with those of HK, however since of the  $1/\cos i$  factor in Eq. (7) we cannot handle the case  $i = 90^\circ$ , while model profiles by HK are only for  $i = 90^\circ$ .

To overcome these difficulties for the comparison we construct a quadratic extrapolated shell profile for  $i = 90^\circ$  using the calculated shell profiles at reliable inclinations  $76^\circ, 78^\circ$  and  $80^\circ$ . This extrapolation for  $i = 90^\circ$  is also shown in Fig. 3 (dotted line). The comparison with the shell profile, given by HK in his Fig. 8d, clearly shows that the two central depressions match in intensity at  $F = 0.8F_c$  but the central peak in our constructed profile is about 0.13 continuum units too low. This shows that our adapted version of the HM approximation works well for inclinations up to  $i \simeq i_u$ . Only the central part of the profile becomes biased.

The formation of the central peak was predicted and explained by HK and observational aspects were discussed by Rivinius et al. (1999). Our test calculation show that the central peak in the shell profile as a function of inclination is still present at  $i = 70^\circ$ .

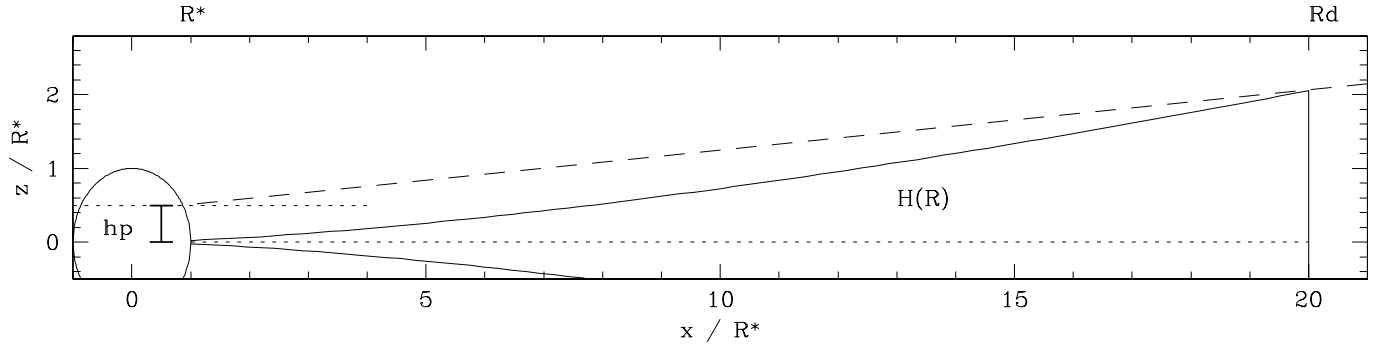


**Fig. 2.** Projection of the disk scale height  $H(R_d)$  onto the star at large inclinations. The shadow height is indicated by  $h_p$ .

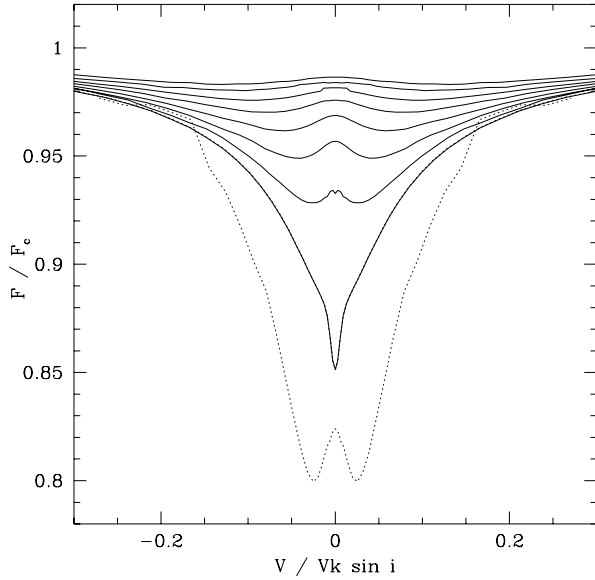


**Fig. 3.** Pure shell absorption profiles for Fe lines ( $V_{th} = 1.7 \text{ km s}^{-1}$ ) at inclinations  $i = 70^\circ, 72^\circ, 74^\circ, 76^\circ, 78^\circ, 80^\circ, 82^\circ$  and  $84^\circ$ . Profiles at  $i = 82^\circ$  and  $i = 84^\circ$  are no longer reliable since the critical inclination for these model parameters is  $i_c = 87$ . The dotted shell profile gives the estimated result for  $i = 90^\circ$ . It is constructed with profiles at  $i = 76^\circ, 78^\circ$  and  $80^\circ$  via a quadratic extrapolation

### 3. Model line profiles

#### 3.1. Shear broadening

Shear broadening is an anisotropic scattering process and is able to deepen the central depression with respect to the peak intensity under certain conditions (Fig. 4, Fig. 5). Profiles in Figs. 4 and 5 have been continuum subtracted and normalized to  $F_{max} = 1$ . The velocities are normalized to the current maximum kinematical broadening given by  $V_K \sin i$ . In both cases the total width of calculated emission lines is mainly determined by the maximum kinematical broadening  $V_K \sin i$ . Consequently, the normalized total width  $\Delta V_{tot}/V_K \sin i$  and the normalized peak separation  $\Delta V_p/V_K \sin i$  are retained for a large range of inclinations. The large thermal velocity  $V_{th} = 13 \text{ km s}^{-1}$  makes it difficult for the local velocity shear to exceed the first term in Eq. (9) and to lower the central depression, which is only

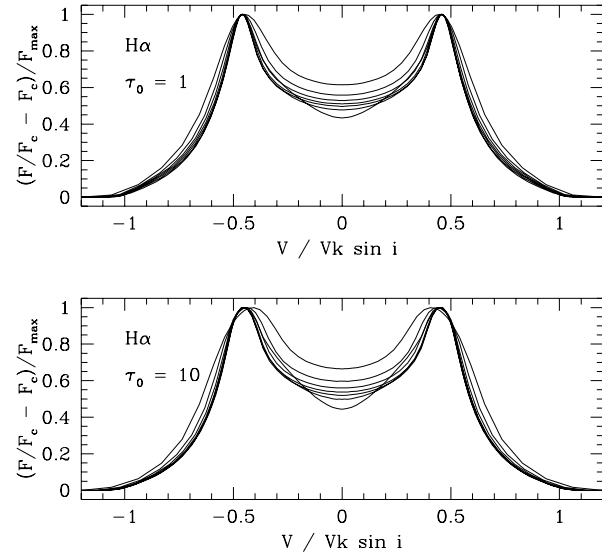


**Fig. 4.** Series of continuum subtracted emission line profiles with  $i = 20^\circ, 30^\circ \dots 80^\circ$ . The profiles are normalized to  $F_{max} = 1$  and the velocities are given in units of  $V_K \sin i$ . The intrinsic isotropic broadening is  $\Delta V_{th} = 13 \text{ km s}^{-1}$ , typical for hydrogen at  $T = 10\,000 \text{ K}$ . Upper panel for  $\tau_0 = 1$ ; lower panel for  $\tau_0 = 10$ .

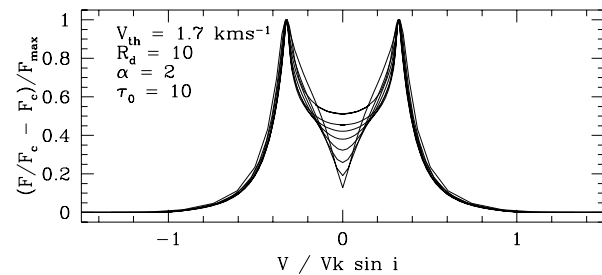


**Fig. 5.** Series of continuum subtracted emission line profiles with  $i = 10^\circ, 20^\circ, 30^\circ \dots 80^\circ$ . The profiles are normalized to  $F_{max} = 1$  and the velocities are given in units of  $V_K \sin i$ . The intrinsic isotropic broadening is  $\Delta V_{th} = 1.7 \text{ km s}^{-1}$ , typical for Fe at  $T = 10\,000 \text{ K}$ .

$F_{cd}/F_{max} = 0.5$  at  $i = 80^\circ$ . Much deeper central depressions occur for emission lines with small intrinsic broadening, as is shown for Fe line profiles ( $V_{th} = 1.7 \text{ km s}^{-1}$ ) in Fig. 5.

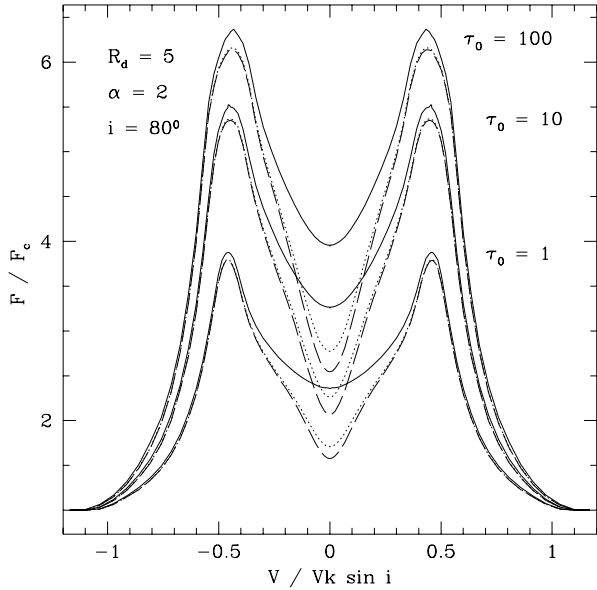


**Fig. 6.** Impact of stellar obscuration and shell absorption on circumstellar H $\alpha$  ( $V_{\text{th}} = 13 \text{ km s}^{-1}$ ) emission line profiles for different values of  $\tau_0$ . Solid profiles: No stellar obscuration and no shell absorption; Dotted profiles: Stellar obscuration but no shell absorption; Dashed profiles: Shell absorption and stellar obscuration are taken into account.

### 3.2. Stellar obscuration

The influence of stellar obscuration upon the line profile is demonstrated in Fig. 6 for a disk with  $R_d = 5$  at  $i = 80^\circ$ , and for different values of  $\tau_0$ .

For  $R_d = 5$  the obscuration radius  $R_o(i = 80^\circ) = 5.8$  slightly exceeds the disk radius. Therefore, the rear radial velocity branch in the equatorial plane of the disk with  $V_{\text{rad}} = 0 \text{ km s}^{-1}$  is completely obscured by the central star, resulting in a depression down to the half of the unobscured profile. This geometric effect increases with inclination but is independent on  $\tau_0$ . Also the peak intensity is slightly depressed by stellar obscuration.

### 3.3. Shell absorption

Profiles, also affected by shell absorption, are plotted in Fig. 6 as dashed lines. The additional depression is still rather small here at  $i = 80^\circ$  with respect to stellar obscuration. The depression is more concentrated at  $V = 0 \text{ km s}^{-1}$  because of the curves of constant radial velocities, while obscuration is more widely distributed in velocity space.

The same parameter study is performed for emission lines with smaller intrinsic broadening of  $V_{\text{th}} = 1.7 \text{ km s}^{-1}$ . The resulting profiles are given in Fig. 7. The profile series with  $\tau_0 = 0.01$  represents obscuration in the optically thin limit and results in a flat central depression (see also Hanuschik 1987, his Fig. 3). Up to now we assumed that the emissivity, which is parameterized in our model by  $S_0 = \text{constant}$ , has the same radial gradient as the occupation density. However, emission

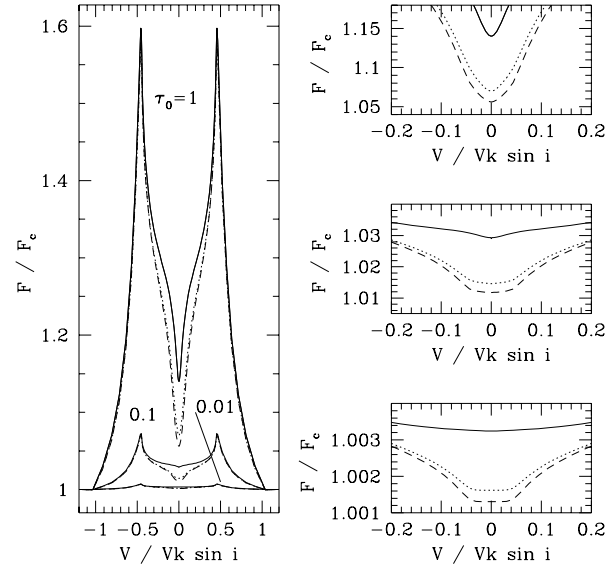


**Fig. 7.** Impact of stellar obscuration and shell absorption on circumstellar Fe II ( $V_{\text{th}} = 1.7 \text{ km s}^{-1}$ ) emission line profiles for different values of  $\tau_0$ . Left panel: Solid profiles: No stellar obscuration and no shell absorption; Dotted profiles: Stellar obscuration but no shell absorption; Dashed profiles: Shell absorption and stellar obscuration taken into account. The three right hand side panels show the zoomed central part of the profiles for  $\tau_0 = 1$  (top),  $\tau_0 = 0.1$  (middle) and  $\tau_0 = 0.01$  (bottom).

equivalent widths of observed H $\alpha$  and Fe II 5317 Å lines usually show a ratio of  $W_\alpha/W_F \approx 100$ . This is because metallic lines are much more optically thin and more dependent on the diluted stellar radiation field. In order to account for the lower source function, we reduce the circumstellar emissivity  $S_0 = 0.5$  by an arbitrary factor of 10, keeping all other parameters fixed. Resulting model profiles are given in Fig. 8 for four values of  $\tau_0$ . The emission profiles are now a factor 10 less intense and shell absorption lowers the central line intensity below the local stellar continuum  $F_c$ .

## 4. Application to observed H $\alpha$ emission lines

### 4.1. Observations

High-resolution observations of H $\alpha$  emission lines have been obtained during several runs at the 2.2m telescope on Calar Alto (Coudé focus f/12 + CCD,  $R = \frac{\lambda}{\Delta\lambda} = 45\,000$ ) and the 1.52m telescope at Observatoire de Haute Provence (Coudé focus, Aurélie spectrograph + one-dimensional CCD (Barette Thomson),  $R = 72\,000$ ) in the context of a survey on the long-term variability of northern Be stars (Hummel & Vrancken 1995). The data reduction includes correction for offset (read-out-noise), flat-fielding, wavelength calibration, removal of terrestrial water vapor lines with a mask obtained from a bright O-type star and a correction of the heliocentric velocity frame. Details can be found in Hummel & Vrancken (1995). From our large sample we selected H $\alpha$  emission lines which fulfill the requirements discussed in Sect. 3.1.2. This includes a max-

**Table 1.** Stellar parameters and adopted parameters to fit the stellar H $\alpha$  absorption profile. The MK-type, the stellar rest velocity  $V_{\text{pec}}$  and  $v \sin i$  are from Hoffleit & Jaschek (1991);  $T_{\text{eff}}$ ,  $\log g$ ,  $M_*$  and  $R_*$  are interpolated from the tables of Allen (1973) or fitted in the case of HR 6984 and HR 7565. The inclination has been estimated assuming  $V_{\text{rot}} = 0.8V_c$ , where  $V_c = \sqrt{GM_*/R_*}$  is the critical or break-up velocity of the star.

HR	MK	$T_{\text{eff}}$ $10^3 K$	$\log g$	$v \sin i$ $\text{km s}^{-1}$	$V_{\text{pec}}$ $\text{km s}^{-1}$	SF <sup>a</sup>	$M_*$ $M_{\odot}$	$R_*$ $R_{\odot}$	$V_c$ $\text{km s}^{-1}$	$i^e$ $^{\circ}$	$i^f$ $^{\circ}$	site obs/mm/yy
985	B2.5V	21	4.0	350	+4	1.00	9.8	5.2	600	47	56	OHP/10/94
1679	B2IVe	24	4.0	336	+15 <sup>b</sup>	1.000	11.3	8.5	500	57	74	OHP/10/94, 12/95
4123	B9V	11	3.7	310	+13	0.970	3.6	2.0	586	41	49	OHP/03/95 <sup>c</sup>
5440	B2IV	24	4.0	330	0	0.990	11.3	8.5	500	46	71	CAT/02/87 <sup>d</sup>
6984	B5V	15	3.8	310	-27	0.995	6.5	3.9	560	44	52	OHP/03/95
7565	B2.5V	21	4.0	281	-31	1.000	9.8	5.2	600	36	42	OHP/03/95
8375	B2.5V	21	4.0	350	-15	0.980	9.8	5.2	600	47	56	CA/11/93

<sup>a</sup> profiles are normalized to the local stellar continuum. The scaling factor SF is introduced to fit the theoretical model profiles in intensity

<sup>b</sup> the nominal value by Hoffleit & Jaschek (1991) is +3 km s<sup>-1</sup>

<sup>c</sup> the same profile shape is also observed on CA/12/94

<sup>d</sup> from Dachs et al. (1992)

<sup>e</sup> assuming  $V_{\text{rot}} = 0.8V_c$

<sup>f</sup> assuming  $V_{\text{rot}} = 0.7V_c$ , according to Porter (1996)

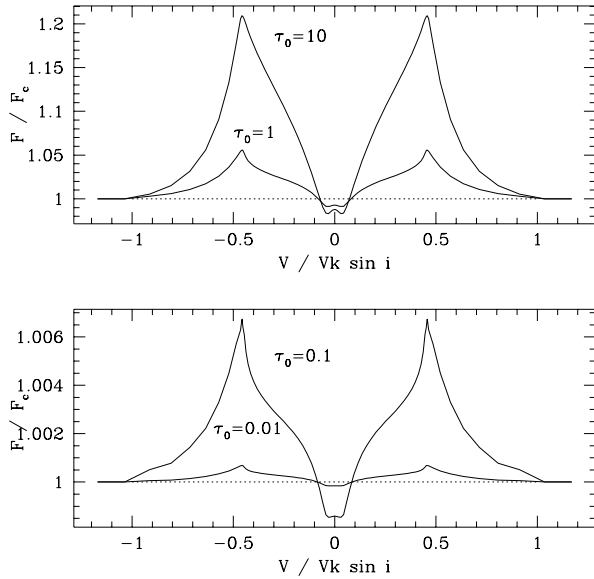


**Fig. 8.** Theoretical profiles as in Fig. 7 except  $S_0 = 0.05$ . Note that the circumstellar emission is low and that, due to shell absorption, the central intensity is below the local stellar continuum

imum equivalent width of  $W_{\text{max}} = 12 \text{ \AA}$  and symmetric (class 1) emission lines. The selected sample is listed in Table 1.

#### 4.2. Subtraction of the underlying stellar absorption profile

For low e.w. emission lines, the underlying stellar absorption profile becomes dominant and has to be subtracted from the observations in order to obtain a net emission profile.

$T_{\text{eff}}$  was taken from the calibration of Allen (1973, p. 206), while for all program stars,  $\log g = 4.0$  was assumed as a first estimate. For each  $(T_{\text{eff}}, \log g)$  pair, photospheric H $\alpha$  line profiles were computed as by Vrancken et al. (1996). In those cases where the underlying absorption is visible in the observations,

$\log g$  was adjusted so that the theoretical absorption profile fitted the observed one. Classical rotational broadening, with  $v \sin i$  from Table 1, together with a velocity shift  $V_{\text{pec}}$  were adopted, and the resulting profile was then subtracted from the observed emission line. In none of the cases  $v \sin i$  or  $V_{\text{pec}}$  have to be modified.

Fig. 9 shows the observed H $\alpha$  profiles together with the adopted rotationally broadened theoretical stellar absorption profiles. The parameters are given in Table 1.

For a number of symmetric H $\alpha$  emission lines (taken from our unpublished archive) with low equivalent width (Fig. 12) we could not find a reasonable fit to the underlying stellar absorption profile within the range of the stellar parameters  $\log g$ ,  $T_{\text{eff}}$  and  $v \sin i$ . The theoretical absorption profile is systematically too low with respect to the observation. We interpret this systematic deviation as a consequence of either electron scattering in the observed emission line or an additional continuum contributed by the disk itself. Since we have no means of estimating these effects those profiles have been excluded from the study.

#### 4.3. Fitting procedure for net emission profiles

To compare observation and theory we assume that the H $\alpha$  occupation density is due to recombination. We therefore modify Eq. (2) with an additional factor of  $\sqrt{\pi}N_e^2$  for  $W$ .

The fits were obtained in several stages. In a first step we calculated model profiles and varied the circumstellar parameters  $n_0$  and  $R_d$  manually until we found reasonable approximation to the observed net emission profile. In a second step, fine-tuning was carried out using a simplex algorithm (Press et al. 1992). To maintain parameter orthogonality we varied  $m$  together with the total number of absorbing particles  $N_d$  and  $V_K$  together with  $V_K \sin i$ . Unless otherwise noted,  $S^L$  is fixed to 0.5.

Net H $\alpha$  emission lines and resulting fits are given in Fig. 9 and in Fig. 10. The adopted parameters of the circumstellar disk are given in Table 2.

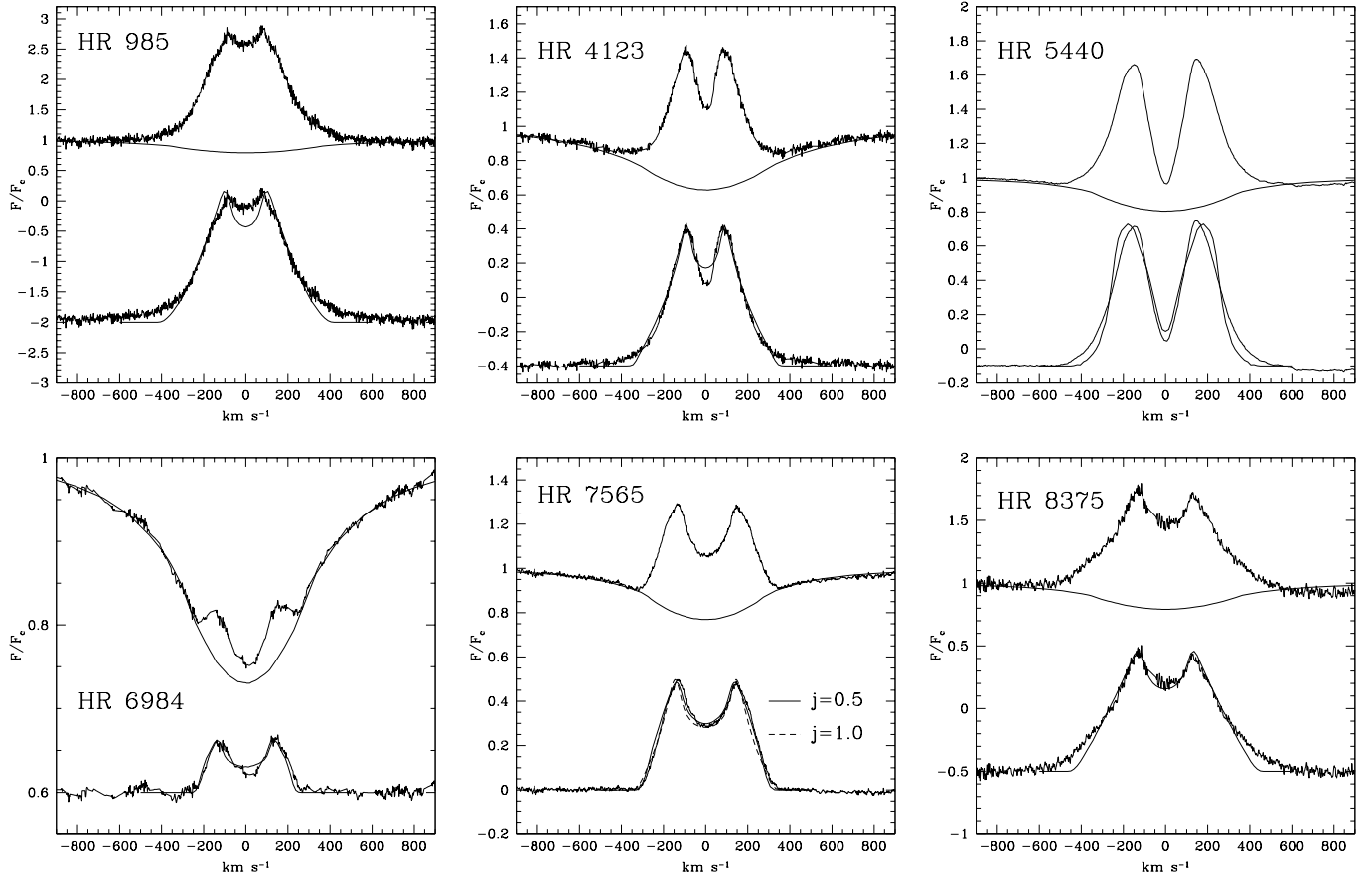


**Fig. 9.** Upper: observed  $H\alpha$  profiles of Be stars and theoretical stellar absorption profiles. Lower: net emission profile and model fit. Stellar parameters of the absorption profile are given in Table 1; best fit parameters for the circumstellar emission are given in Table 2.

### 5. Circular velocity law

Up to now we have assumed Keplerian rotation, but this assumption is still a matter of debate. Usually the radial run of the rotation velocity is parameterized by

$$V_{\text{rot}} = V(R_*)R^{-j}, \quad (18)$$

(e.g. Hutchings 1970), where  $j = \frac{1}{2}$  corresponds to Keplerian rotation and  $j = 1$  corresponds to conservation of angular momentum.

From the correlation of emission line parameters Hanuschik et al. (1988), Mennickent (1991) and Mennickent et al. (1994) found values of  $j \simeq 0.8$ ,  $j \simeq 1.35$  and  $j = 1.4 \pm 0.2$  respectively while Hirata (1994) argued for lower values of  $j$ . Values of  $j \simeq 1$  imply disk formation scenarios due to a continuous mass loss e.g. by a stellar wind. Values of  $j \simeq 0.5$  implies disk formation due to short-term episodic mass-loss events with a fast circularisation and self-accretion (e.g. Kroll & Hanuschik 1997). As an extended parameter study we calculate emission lines with values different from  $j = \frac{1}{2}$  and study the impact on the line shapes. These effects have been investigated by Hutchings (1970) and Hanuschik (1987).

The shear velocity given for  $j = 0.5$  in Eq. (1) is generalized to

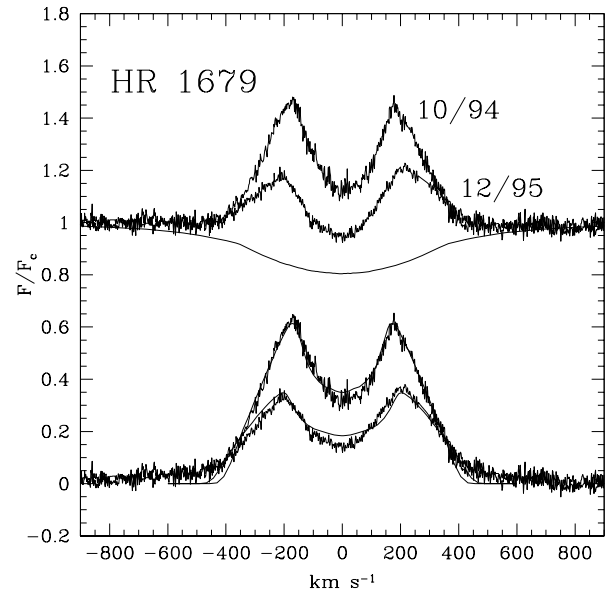


**Fig. 10.** Emission line profiles of HR 1679 ( $\lambda$  Eri), theoretical stellar absorption profile and model fit to the net emission.

$$V_{\text{sh}} = -\frac{jH}{2} V_{\text{rot}} \sin i \tan i \sin \phi \cos \phi. \quad (19)$$

**Table 2.** Final best-fit parameters for the net emission line profiles.  $n_0$  is the foot point equatorial occupation density distribution.  $m$  is the power-law index of the equatorial density occupation density distribution  $n \sim n_0 R^{-m}$ .  $N_d$  is the total occupation number.  $i$  is the inclination.  $V(R_*)$  is the inner rim velocity of the disk.  $R_d$  is the emission disk radius in units of  $R_i$ .

HR	$n_0$ $\text{cm}^{-3}$	$m$	$N_d$ $g$	$i$ $^\circ$	$V(R_*)$ $\text{km s}^{-1}$	$R_d$ $R_*$
985	1005	2.85	1.22e15	48	514	18.5
1679 <sup>a</sup>	214	3.56	9.06e13	57	477	3.56
1679 <sup>b</sup>	148	3.63	4.88e13	57	524	3.63
4123	842	2.69	2.73e14	42	498	16.4
5440 <sup>c</sup>	760	1.62	2.3e15	83	423	5.3
5440	38	2.44	2.6e13	78	405	6.4
6984 <sup>e</sup>	33	2.71	1.03e13	44	325	3.24
7565 <sup>e</sup>	329	2.93	1.34e14	36	493	5.6
7565 <sup>d</sup>	73	2.77	1.09e14	36	534	2.3
8375	575	2.81	5.01e14	47	541	12.7

<sup>a</sup> observation date 10/1994, inclination fixed

<sup>b</sup> observation date 12/1995, inclination fixed

<sup>c</sup>  $S^L = 0.035 F_c$  used

<sup>d</sup>  $j = 1$  fixed,  $i$  fixed,  $n_0$ ,  $V$  and  $m$  varied

<sup>e</sup> inclination fixed

For optically thin line radiation the influence of  $j$  on the line profiles is just a rescaling of the line-of-sight velocity scale. As a representative example we fitted the  $H\alpha$  profile of HR 7565 with  $j = 1$  starting with the best fit parameters for  $j = 0.5$  and varied only  $n_0$ ,  $m$  and  $R_d$ . The resulting emission line is given by the dashed profile in Fig. 9. The final model parameters for the  $j = 1$  model disk are given in Table 2. The resulting disk size is smaller and the parameterized density is lower with respect to the Keplerian fit.

In the optically thick case, where  $\tau$  is dependent on the local velocity shear (i.e. on the radial gradient of the rotation velocity; see Eq. 7),  $j = 1$  will result in a larger velocity shear for  $R < 2$  and a lower velocity shear for  $R > 2$  with respect to Keplerian rotation ( $j = 0.5$ ). In Fig. 11, a series of optically thick model profiles with variable  $j$  is shown. The parameters are identical to the best-fit model for HR 5440 except that a slightly lower inclination of  $i = 80^\circ$  has been taken.

## 6. Discussion

The results presented in Fig. 9 and in Fig. 10 show that we have found reasonable fits for our selected set of low equivalent width symmetric  $H\alpha$  net emission. In particular for the two Be stars of later spectral type like HR 4123 the Balmer lines are the only available emission lines to study the structure of Be star disks. In the case of HR 6984  $H\alpha$  is the only spectral trace of an circumstellar disk at all.

In the optically thin case, the parameterized number occupation density  $n_0$  and the emission strength ratio with respect to the local stellar continuum  $S^L$  both control the intensity of the theoretical emission lines.  $S^L$  has been kept fixed to  $S^L = 0.5$ . The best fit value of  $n_0$  also compensates for the unknown line

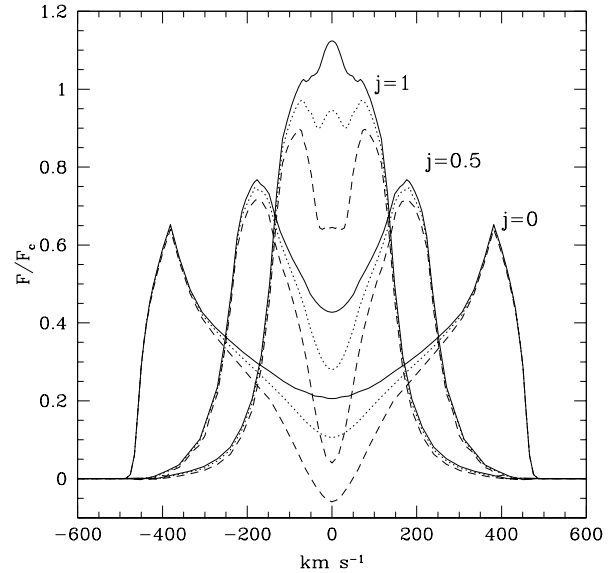


**Fig. 11.** Series of  $H\alpha$  model profiles with variable velocity field  $V_{\text{rot}} = 423 \text{ km s}^{-1} R^{-j}$ .  $j = 1$  corresponds to conservation of angular momentum,  $j = 0.5$  corresponds to Keplerian rotation. The notation is as in Fig. 4: solid line without shell absorption and stellar obscuration, dotted line: with stellar obscuration, dashed line: both effects taken into account.

emission strength and cannot be associated with a real occupation density.

A similar behavior is known for the inclination  $i$  and the radial velocity  $V_K$ . Only the product  $V \sin i$  can be derived from optically thin line profiles. This situation is matched by most of our model fits, hence the resulting inclinations given in Table 2 are close to the initial values given in Table 1. Admittedly our individual results for  $V_K$  are dependent on the initial value of  $i$ . Using  $V_{\text{rot}} = 0.7V_c$  as proposed by Porter (1996) the larger initial inclination given in column 12 of Table 1 would result in lower values of  $V_K$  but would not impact the disk radius  $R_d$ . For nearly edge-on view the inclination dependent absorption processes can be used to constrain  $i$  apart from the initial estimate. This is demonstrated by the multi-parameter fit for HR 5440 where an inclination of  $= 83^\circ$  is required while the estimated initial inclination is  $i = 46^\circ$  assuming  $V_{\text{rot}} = 0.8V_c$ .

Radial runs of the occupation density are found to range from  $m = 2.7$  to  $m = 3.6$  for our optically thin profiles. The nearly shell star HR 5440 requires  $m = 1.6$  to fit the deep central profile depression. The  $H\alpha$  emitting disk as derived from the model fits range from  $R_d = 3.5$  for HR 1679 to  $R_d = 18.5$  for HR 985.

For HR 5440 the theoretical net emission is not sufficiently depressed in the center with respect to the observations. For this star we also allowed  $S^L$  to be a free parameter. A value of  $S^L < 0.5$  requires a larger  $n_0$ , hence a larger optical depth deepens the central line intensity with respect to the peaks. For HR 5440 we find a reasonable fit, assuming the line source function of  $H\alpha$  to be about 3% of the local stellar continuum.

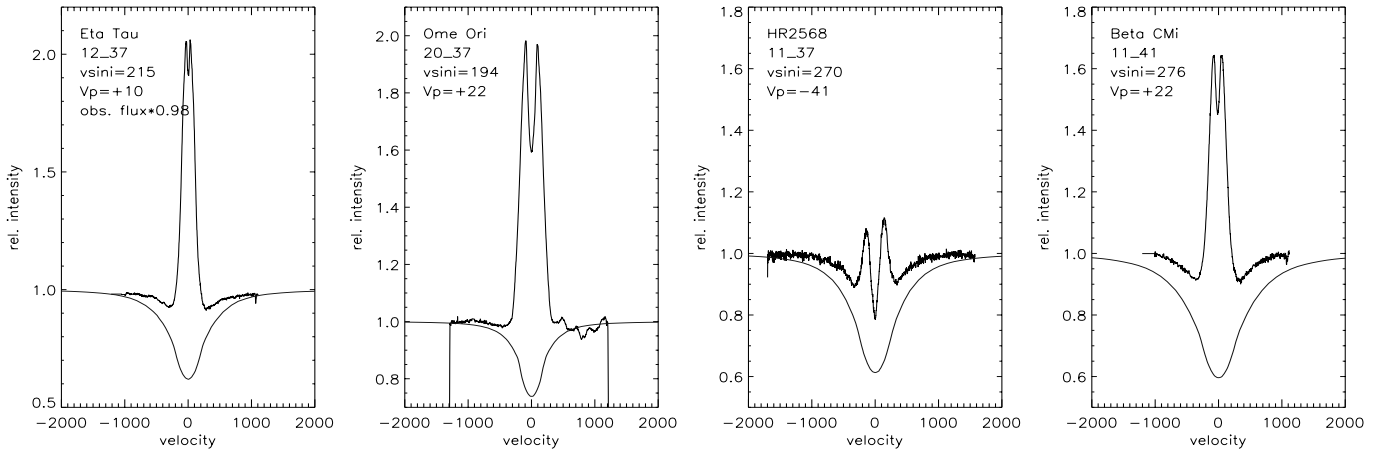


**Fig. 12.** Observed  $H\alpha$  emission line profiles for which no satisfactory fit for the stellar absorption profile could be achieved. Stellar fit parameters for effective temperature  $T_{\text{eff}}$ , gravitation  $\log g$ , stellar rotation  $v \sin i$ , and rest frame velocity  $V_p$  are given in each individual plot. From left to right:  $\eta$  Tau (=HR 1165),  $\omega$  Ori (=HR 1943), HR 2568 and  $\beta$  CMi (=HR 2845). net emission.

HR 1679 ( $\lambda$  Eri) is known to experience episodic emission events. The emission steadily increased from Jan 1994 on (Štefl 1994) and faded again after Oct 1994. Both net emission profiles of HR 1679 (see Fig. 10) could be reproduced. The model parameters indicate that the reduction in the emission is due to the decreasing density in the disk; the emission radius remained constant (Table 2).

Optically thin profiles contain insufficient information to constrain the rotational parameter  $j$ . The two fits of HR 7565 demonstrates this ambiguity. However, for large inclinations and/or large optical depth,  $j$  has a strong influence on the line shape as demonstrated in Fig. 11. First the peak separation increases with decreasing  $j$ . This is the trivial effect also occurring in the optically thin limit. Secondly the line-of-sight velocity range for shell absorption and stellar obscuration ( $R(\phi) < R_o(\phi)$ ) is also increasing with decreasing  $j$ . This can be seen in Fig. 11, where the dashed line and the solid line deviate at different velocities for the given values of  $j$ . The most diagnostic influence comes from the velocity shear. The shear velocity, and hence the anisotropic self absorption in the disk decreases with increasing  $j$ . The radial gradient of the circular velocity is  $-R^{-2}$  for  $j = 1$  and is  $-\frac{1}{2}R^{-\frac{3}{2}}$  for  $j = 0.5$ . Hence the velocity shear is smaller for all  $R > 4$  at  $j = 1$  with respect to  $j = 0.5$  and anisotropic self-absorption decreases with increasing  $j$ . For our example profiles in Fig. 11 shear broadening has vanished for  $j = 1$  and even shell absorption and stellar obscuration are insufficient to produce a central depression comparable to the case of  $j = 0.5$ . The reduction in the velocity shear due to large values of  $j > 0.5$  prevents the formation of deep central reversal between the double peaks of the profiles. The case of  $j = 0$  does not represent a parameterization of a simple physical scenario, it has been included for diagnostic reasons. For  $j = 0$  each annulus of the disk has the same line-of-sight velocity as the innermost annulus at  $R = R_*$ . Consequently  $V_\phi(R_d) = V_\phi(R_*)$  and the whole disk behaves like an optically thick but geometrically narrow ring.

As a further test and in order to establish our result we tried to fit the net emission of HR 5440 (the dashed profile for  $j = 0.5$  in Fig. 11) by keeping  $j = 1$  (as had been done for HR 7565) and  $j = 0.7$  fixed and varied  $n_0$ ,  $m$ ,  $R_d$ ,  $i$  but no model profile was found showing the same deep depression as for  $j = 0.5$ . These results clearly show that the radial distribution of the circular velocity in HR 5440 is in much better agreement with Keplerian rotation ( $j = 0.5$ ) than with conservation of angular momentum ( $j = 1$ ).

## 7. Conclusions

We have adapted the Horne & Marsh (1986) model for  $H\alpha$  emitting disks around Be stars. The impact of the central star's finite size on the line formation process is taken into account. Our model fits to symmetric  $H\alpha$  emission lines of low equivalent width show that these lines can be used to constrain the circumstellar structure for a wide range of disk parameters. In particular at large inclinations opacity effects provide additional constraints to derive the inclination  $i$  the absolute emissivity  $S_0$  and the rotational parameter  $j$ . Although HR 5440 is not classified as a Be-shell star the impact of shell absorption and stellar obscuration is dominant in the  $H\alpha$  line formation.

We investigated the rotational velocity law in Be star circumstellar disks and found that shear broadening becomes less efficient for  $j > 0.5$ . In application to the  $H\alpha$  profile of HR 5440 the rotational parameter can be constrained to  $j = 0.5$ . If we consider Be stars with shell profiles to be not physically different from Be stars without shell characteristics, but rather Be stars seen at high inclinations, our results suggest that the circumstellar disks of Be stars (with symmetric and low equivalent width emission lines) in general rotate in a Keplerian manner.

*Acknowledgements.* Financial support by the *Service Centres and Research Networks* initiated and financed by the Belgian Federal Scientific Services (DWTC/SSTC) project number SC/005 is gratefully acknowledged. M.V. acknowledges financial support by the DWTC/SSTC. Computations have been carried out on workstations,

partially financed by the *FWO* and on the workstation cluster of the Leibniz Rechenzentrum München. This research made use of the Simbad database, operated at the CDS, Strasbourg, France.

## References

- Allen C.W., 1973, *Astrophysical Quantities*, third Ed., Athlone, London
- Dachs J., Hummel W., Hanuschik R.W., 1992, *A&AS* 93, 116
- Hanuschik R.W., 1987, *A&A* 190, 187
- Hanuschik R.W., 1995, *A&A* 295, 423 (HK)
- Hanuschik R.W., 1996, *A&A* 308, 170
- Hanuschik R.W., Kozok K., Kaiser D., 1988 *A&A* 189, 147
- Hoffleit D., Jaschek C., 1991, *The Bright Star Catalogue*, fifth Ed. New Haven, Connecticut: Yale University Observatory
- Horne K., 1995, *A&A* 297, 273
- Horne K., Marsh T.R., 1986, *MNRAS* 218, 761 (HM)
- Hummel W., 1994, *A&A* 289, 458
- Hummel W., 2000, in *IAU Coll. 175*, in press
- Hummel W., Vrancken M., 1995, *A&A* 302, 571
- Hutchings J.B., 1970, *MNRAS* 150, 55
- Hirata R., 1994, *Be Star Newsletter* 29, 10
- Kroll P., Hanuschik R.W., 1997, in: *IAU Coll. 163*, p. 494
- Marsh T.R., 1987, *MNRAS* 228, 779
- Mennickent R.E., 1991, *A&A* 88, 1
- Mennickent R.E., Vogt N., Barrera L.H., Covarrubias R., Ramirez A., 1994, *A&AS* 106, 427
- Poeckert R., Marlborough J.M., 1979, *ApJ* 233, 259
- Poeckert R., Marlborough J.M., 1982, *ApJ* 252, 196
- Porter J.M., 1996, *MNRAS* 280, L31
- Press W.H., Teuholsky S.A., Vetterling W.T., Flannery B.P., 1992, *Numerical Recipes in Pascal*, 2nd Ed., Cambridge University Press
- Rivinius Th., Štefl S., Baade D., 1999, *A&A* 348, 831
- Smith M., Henrichs H.F., Fabregat J. (eds.) 2000, *The Be Phenomenon in Early-Type Stars*, *IAU Coll. 175*, 2000, in press
- Sobolev V.V., 1960, *Moving envelopes*, Harvard University Press
- Štefl S., 1994, *Be Star Newsletter* 28, 5
- Struve O., 1931, *ApJ* 73, 94
- van Kerkwijk M.H., Waters L.B.M.F., Marlborough J.M., 1995, *A&A* 300, 259
- Vrancken M., Butler K., Becker S., 1996, *A&A* 331, 661
- Waters L.B.M.F., 1986, *A&A* 162, 121